Progress In Electromagnetics Research M, Vol. 119, 161–175, 2023

A Compact Low-Profile P-Shaped Wearable Antenna for Medical Application

Zainab Yunusa*

Abstract—This research article introduces a compact wearable antenna designed specifically for medical applications. The antenna underwent prototyping using a flexible Rogers Duroid RO3003$^{\text{TM}}$ material, featuring a small form factor measuring $35 \times 32 \times 0.5\,\text{mm}^3$. In the initial phase of the design process, a basic P-shaped rectangular patch antenna was employed. However, during the first design iteration (Design 1), the antenna demonstrated a single resonance around 1.2 GHz, although it was not optimally matched at that frequency. To tackle this problem and achieve miniaturization involved the introduction of two rectangular patches positioned below the P-shaped patch known as Design 2. To further improve its performance, an inverted L-slot was incorporated. The frequency of operation for the antenna is 2.4 GHz, with a bandwidth measuring 25.2% ranging from (2.087–2.692) GHz. The measured radiation patterns demonstrate bidirectional properties in the E-plane and omnidirectional properties in the H-plane and maintain a high gain of 3.54 dBi and an efficiency of 91%. The SAR values are 0.018/0.013 Watt/kg on the chest. Similarly, the SAR values are 0.02/0.015 Watt/kg on the thigh, using 1/10 g of human tissue, which comply with the standards set by the FCC and the ICNIRP. Furthermore, the simulation and measurement under bending investigation and being close to the human body demonstrate excellent performance. Therefore, the suggested antenna holds significant potential as a compact solution for wearable medical applications.

1. INTRODUCTION

Body-Centric Wireless Communication (BCWC) has become increasingly essential in wearable technology, particularly in the fields of telemetry and healthcare [1, 2]. BCWC enables the monitoring of patients' health conditions, whether they are at a residential setting, medical center, or undergoing non-residential procedures through the utilization of embedded and wearable systems, and BCWC allows for constant and inconspicuous surveillance of various vital signs, including thermometry, arterial pressure, and cardiac rhythm [3]. The effectiveness of BCWC is strongly dependent on the performance of the wireless modules. These devices must possess characteristics such as lightweight design, compact, adaptability to the human body's shape, and the ability to provide uninterrupted surveillance [4].

BCWC operates within different frequency ranges depending on the specific application. For medical implant communications networks, the assigned frequency is 400 MHz. Industrial, scientific, and medical (ISM) applications utilize frequencies of 2.4 GHz and 5.8 GHz. Ultra-wideband (UWB) services operate within the frequency range of 3 GHz to 10 GHz [5, 6].

Antennas for wearable application are essential to the body-worn systems since it is in charge of sending and receiving signals from the embedding equipment and body-worn systems. Therefore, in contrast to antennas installed in off-body, the performance may be impacted. The lossy and inhomogeneous interface to the human physique is mostly responsible for this [7–9].

Received 13 July 2023, Accepted 2 September 2023, Scheduled 7 October 2023
* Corresponding author: Zainab Yunusa (zee2yunusa@gmail.com).
The author is with the Department of Electrical Engineering, University of Hafr Al Batin, Hafr Al Batin, Saudi Arabia.

To maximize efficiency, antenna optimization is essential since the human physique acts as a medium that hampers electromagnetic wave transmission. A significant amount of these waves are taken into the body, which converts the waves into heat energy [10–12].

In addition, it is essential to take into account the impact of antennas on human tissues, which could be assessed by considering the Specific Absorption Rate (SAR) limits. Compliance with these limits is mandated by both the Federal Communications Commission (FCC) and the International Commission on Non-Ionizing Radiation Protection (ICNIRP) standards [13, 14]. Simultaneously, it is necessary to exercise caution regarding the antenna's dimensions, aiming to minimize it as much as possible. Hence, wearable antenna design has been considered an undertaking that is challenging. Over the past few years, numerous configurations of flexible/wearable antennas were investigated, including patch antenna [15, 16], monopole [17, 18], planar inverted F-shape antenna (PIFA) [19], fractal antenna [20, 21], reconfigurable antenna [7, 22], and Substrate-Integrated Waveguide (SIW) [23].

In the past, multiple varieties of wearable antennas have been developed. In [24] a fractal antenna was created specifically for 2.4 GHz applications. Nonetheless, interaction with the human body may result in resonance alteration, thereby negatively impacting the antenna's performance, resulting in impedance mismatch within the desired frequency range. A compact dimension coplanar waveguide (CPW) antenna has been designed [25]. Also this design suffers from a limited bandwidth. In [26], a monopole antenna for wearable devices has been designed and fabricated, utilizing fabric material as the substrate. This design is specifically intended for wireless body area network (WBAN) applications. In [27], an ISM band wearable antenna incorporating a graphene sheet has been designed. Reducing the size of wearable antennas while preserving satisfactory antenna performance has consistently posed a challenge. Various approaches were explored for making wearable antennas compact in dimension, including the implementation of shorting pins [28, 29], quarter mode designs [30, 31], high permittivity materials [32, 33], and reactive loading [34]. By employing the aforementioned techniques, antenna dimensions were noticeably decreased.

Notwithstanding, these antenna designs possess several limitations, including large physical dimensions, narrow bandwidth, low gain, increased back radiation, and restricted suitability for medical because of the inflexible characteristics of the utilized materials. Using flexible RT/duroid 3003 material in this study has successfully tackled the challenges related to the rigidity and inflexibility of typically traditional antennas.

A compact low-profile P-shaped wearable antenna for medical applications is presented in this study. Section 2 of the study discusses the antenna's configuration and parametric investigation. Analysis of the antenna's radiation characteristics is presented in Section 3, while Section 4 focuses on the bending analysis. The antenna's performance in proximity to the human body is examined in Section 5, followed by an exploration of the SAR calculation detailed in Section 6. Table 1 presents a comparative analysis between the suggested antenna and prior literature. Finally, Section 7 presents the conclusion.

2. ANTENNA DESIGN AND APPROACH

2.1. Antenna Configuration and Size

Initially, the antenna's design specifications are determined by adopting the basic microstrip-fed antenna. Subsequently, the patch's dimensions, including its length and width, are computed utilizing the transmission line model as outlined in [35]. To assess variations in the dimensions surrounding the radiating plane and parameters optimization, the CST MWS software is employed. The initial stage of the design process involved a basic P-shaped rectangular patch antenna. In this first design iteration (Design 1), the antenna exhibited a single resonance around 1.2 GHz, but it was not properly matched at that frequency. To address this issue and achieve miniaturization, the introduction of two rectangular patches positioned below the P-shaped patch known as design 2 was involved. Further enhancements were made by incorporating an inverted L-slot, leading to the proposed design. The introduction of slots to the radiating structure and incorporation of a partial ground leads to enhanced compactness and expanded bandwidth. A flexible RT/duroid 3003 material with a loss tangent coefficient of 0.0013, a dielectric constant of 3, and a depth of 0.5 mm is utilized as a substrate. Fig. 1 illustrates the evaluation process of the P-shaped, additionally etched with an inverted L-slot with a CPW feeding structure.

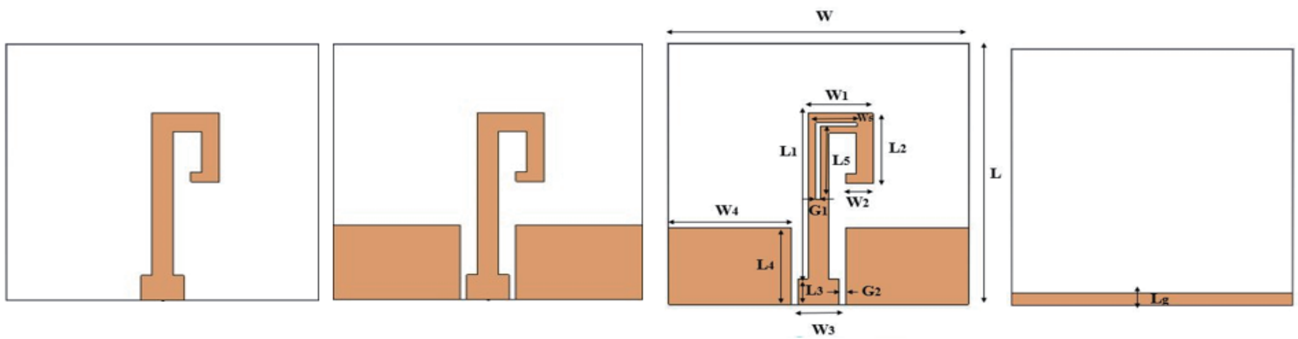

(a) (b) (c) (d)

Figure 1. Proposed design development: (a) design 1, (b) design 2, (c) proposed antenna, (d) back Antennas dimensions are $L = 35\,\mathrm{mm}$, $W = 32\,\mathrm{mm}$, $W1 = 9.9\,\mathrm{mm}$, $L1 = 23\,\mathrm{mm}$, $W2 = 3\,\mathrm{mm}$, $L2 = 11\,\mathrm{mm}$, $W3 = 2.8\,\mathrm{mm}$, $L3 = 2.5\,\mathrm{mm}$, $h = 0.5\,\mathrm{mm}$, $W4 = 13\,\mathrm{mm}$, $L4 = 12\,\mathrm{mm}$, $L5 = 14.2\,\mathrm{mm}$, $W5 = 6\,\mathrm{mm}$, $G1 = 0.5\,\mathrm{mm}$, $G2 = 0.75\,\mathrm{mm}$, $Lg = 2\,\mathrm{mm}$.

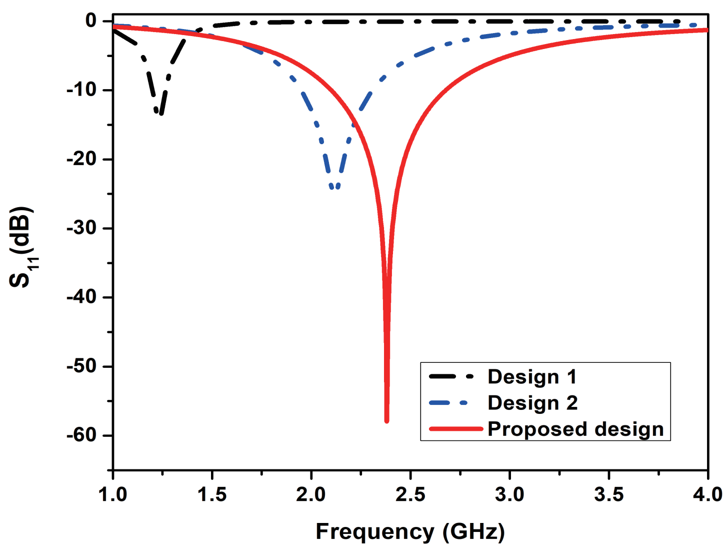

Figure 2. S_{11} simulation for the design development process.

The overall dimension of $35 \times 32 \times 0.5\,\mathrm{mm}^3$ ($0.28\lambda_0 \times 0.27\lambda_0 \times 0.004\lambda_0$) was chosen. Fig. 2 depicts a comparison of the simulated reflection coefficients (S_{11}) at different design processes.

2.2. Parametric Investigation

To examine the influence of alterations on the antenna's performance, a thorough investigation was carried out, involving a parametric study. The objective was to identify the most suitable dimensions for the two patches positioned below the radiating plane (referred to as $L4$ and $W4$ in Figs. 3(a) and (b), respectively). Additionally, an analysis was conducted to evaluate the influence of different ground plane structures, denoted as Lg, as depicted in Fig. 4. The range of Lg variations spanned (35–2.0) mm. Through parametric investigation, it was determined that Lg should be set at 2 mm, indicating that the antenna operates with a defective ground structure rather than a complete one. Moreover, the dimensions ($L5$ and $W5$) of the inverted L-slot on the patch were found to significantly impact the operating band. Therefore, a separate parametric investigation was performed to determine the optimal dimensions of the inverted L-slot on the radiating element. The outcomes of this study

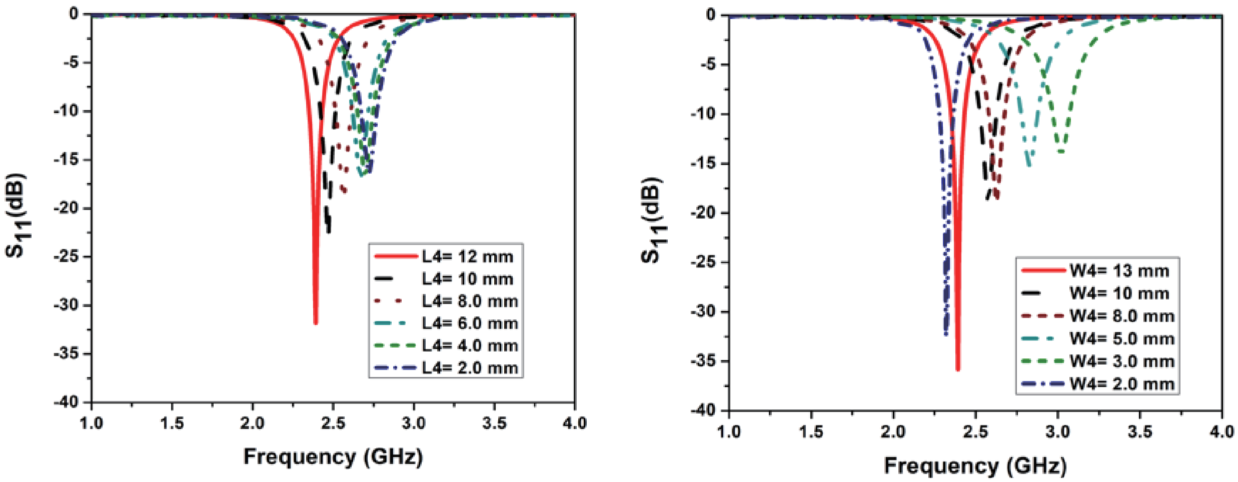

(a) (b)

Figure 3. Variation in the S_{11} (a) $L4$ (b) $W4$.

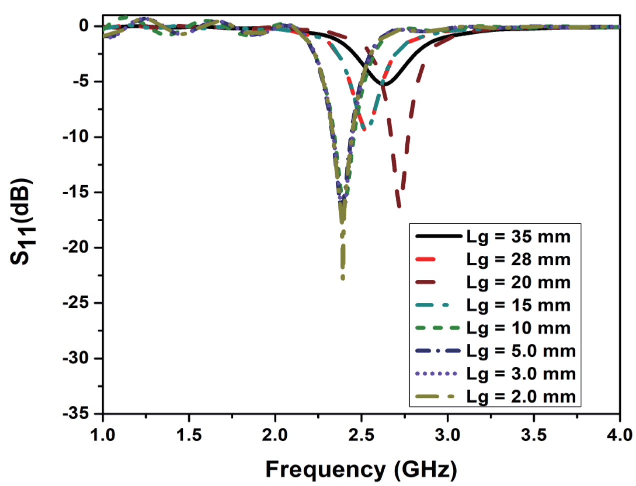

Figure 4. Variation in the S_{11} to the ground structure length.

are presented in Figs. 5(a) and (b). Altering the dimensions of the inverted L-slot affects the resonant frequency. Specifically, adjusting within the range of (1.0–10) mm led to a change in the operating frequency from approximately 2.0 to 3.0 GHz.

3. RESULTS AND ANALYSIS

The fabricated antenna was used for verifying the suggested design, which can be observed in Fig. 6(a). An obtainable 50 Ω SMA connector is employed to connect the antenna. Keysight's Vector Network Analyzer (VNA) PNA-L was used for measuring the antenna performance, as depicted in Fig. 6(b). S_{11} was examined both through simulation and measurement. The findings are illustrated in Fig. 7. The measured results exhibit a slight frequency deviation, which may be faulted in fabrication defects and measurement disparities. The simulated outcome indicates a bandwidth of 25.2% spanning (2.087–2.692) GHz, while the measured result shows a bandwidth of 21.4% spanning (2.079–2.613) GHz. These measurements align quite well with the computational results. The figure illustrates a satisfactory correlation between the S_{11} results obtained from the simulation and the actual measurement.

Figure 8 illustrates the antenna's current distribution. The simulations were conducted at 2.4 GHz

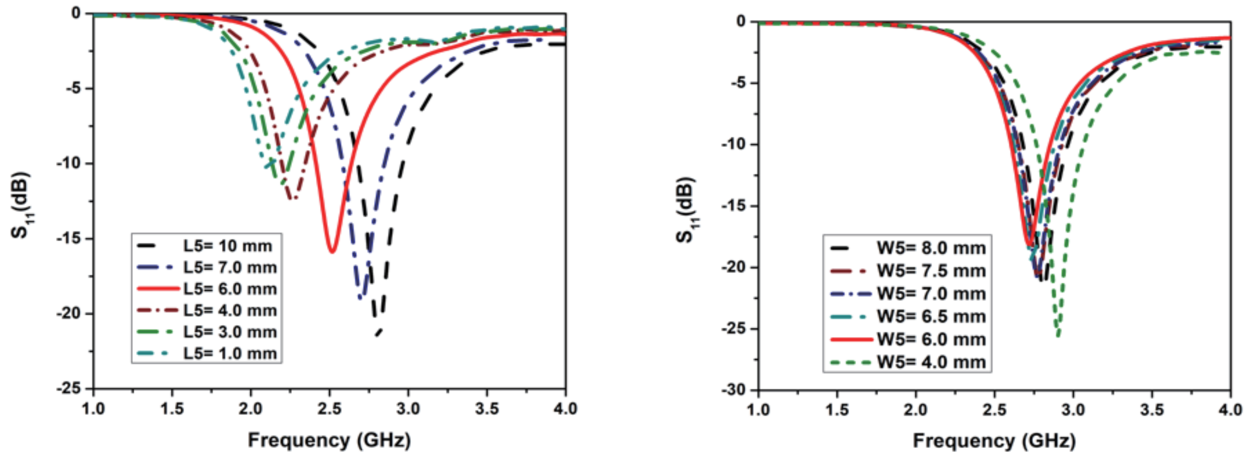

(a) (b)

Figure 5. Variation in the S_{11} (a) $L5$ (b) $W5$.

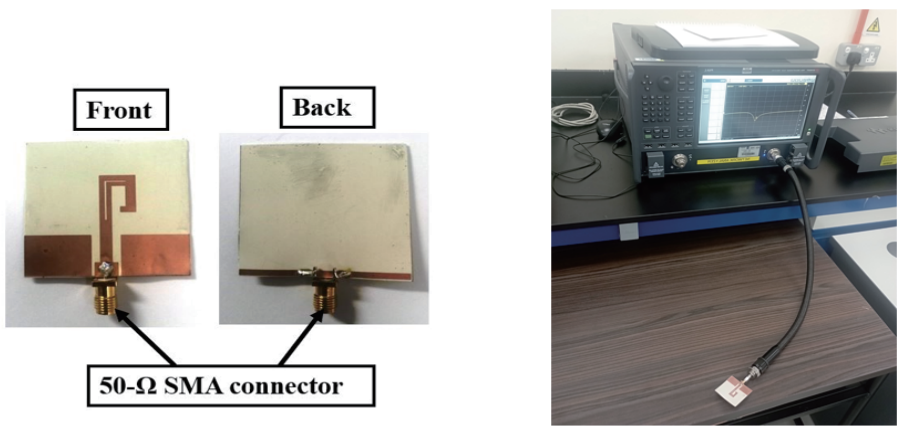

(a) (b)

Figure 6. (a) prototype antenna (b) S_{11} measurement setup.

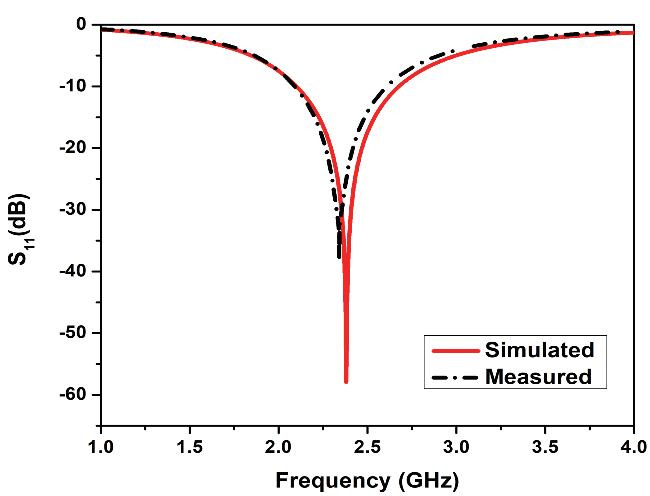

Figure 7. S_{11} comparison.

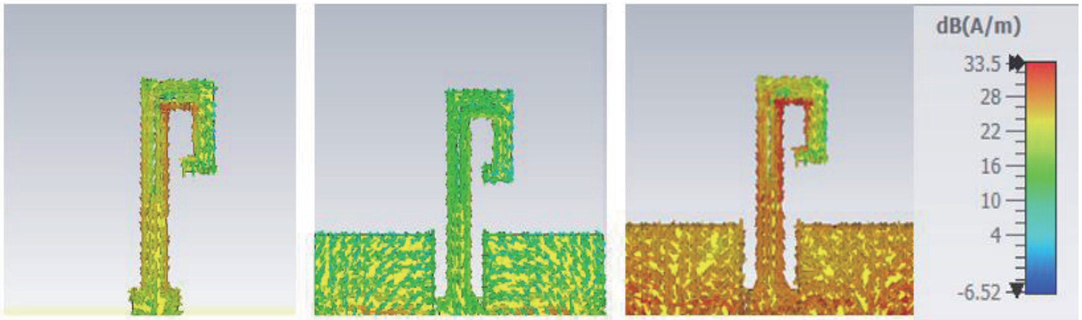

(a) (b) (c)

Figure 8. Current distributions on (a) design 1 (b) design 2 (c) proposed antenna.

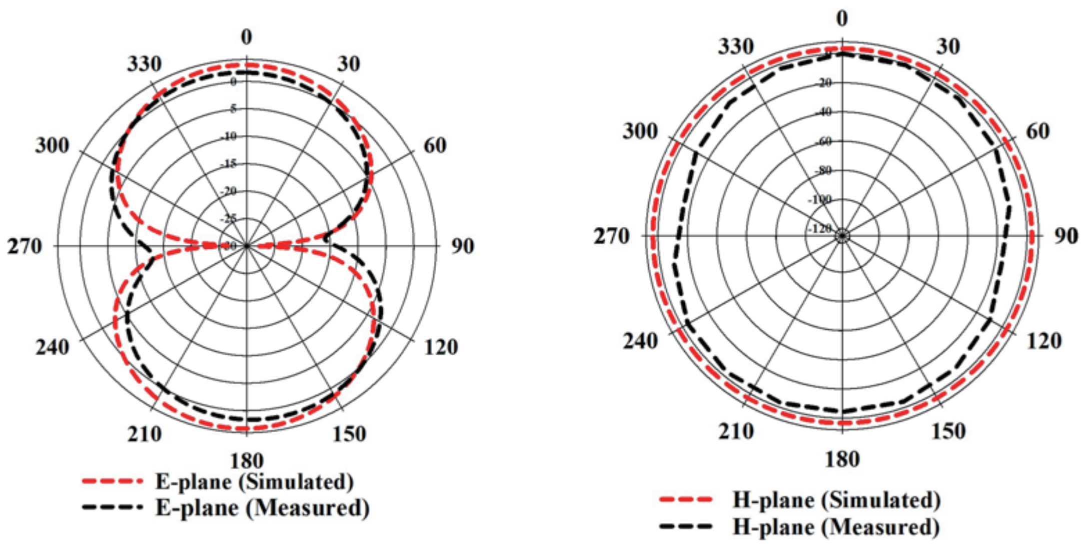

(a) (b)

Figure 9. Radiation patterns (a) E plane (b) H plane.

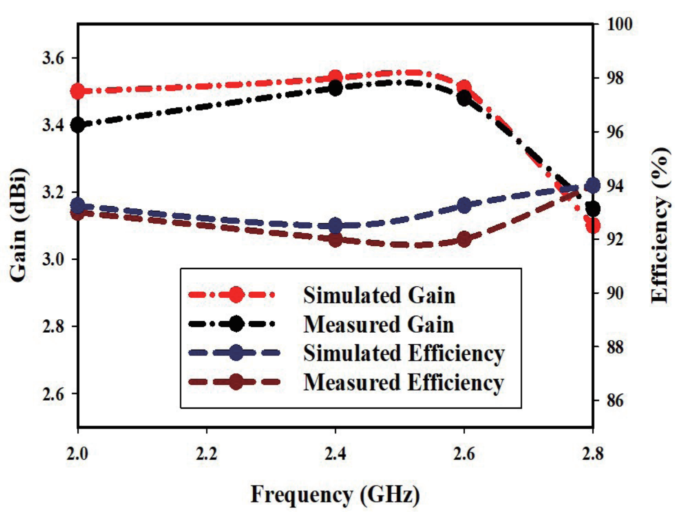

Figure 10. Gain vs efficiency of the proposed antenna.

for three designs: design 1, design 2, and the suggested design. The evidence is clear that the current distribution is lower in the situations of designs 1 and 2, whereas it is highly concentrated with the suggested design. This observation suggests combining a P-shaped that has an inverted L-shape and two patches efficiently diverts and expands the current flow. As a result, this variation in the current flow induced the frequency to decrease, moving from a higher frequency to a lower one.

Figure 9 illustrates the radiation patterns of the antenna, in the E-plane and H-plane. The results demonstrate a satisfactory agreement between the two sets of data. Additionally, the radiation patterns in the E-plane exhibit nearly bidirectional characteristics as depicted in Fig. 9(a), while omnidirectional characteristics in the H-plane are showcased as shown in Fig. 9(b). It is worth noting that the radiation patterns in both planes have been normalized for comparison purposes. Furthermore, the proposed antenna is capable of operating within the 2.4 GHz ISM band. Fig. 10 illustrates that it achieves a gain of 3.54 dBi and an impressive efficiency of 91% in the resonant frequency.

4. BENDING INVESTIGATION

In several applications, wearable antennas are anticipated to adapt to the contours of the human body and remain resilient when being subjected to bending during their operation. This necessitates investigation under bending conditions, particularly for medical applications. Therefore, prior to studying the influence of body tissue loading, it is necessary to examine the performance under various levels of the framework in an unobstructed environment to ensure its consistency. Two orientations, namely vertical and horizontal, were considered and experimentally tested as depicted in Figs. 11(a)–(d). Bending experiments were performed using different diameters (d) (60, 90, 100, and 130) mm representing a range of sizes for the human body. Figs. 12(a)–(d) present the simulated and measured S_{11} characteristics under vertical and horizontal directions, respectively. In each instance, there is a minor upward shift observed with increasing diameter. The simulation results show considerable precision as compared with the measured one, which may be faulted in fabrication defects and measurement disparities. Additionally, the radiation patterns were examined through simulation for the four different diameters, while the measurement is conducted using a 130 mm, as depicted in Figs. 13(a) and (b). The radiation pattern remains uniform with various diameters, exhibiting no distortion at 2.4 GHz in the horizontal and vertical orientations. Moreover, a decrease is observed in the antenna's gain when being subjected to bending conditions, as illustrated in Fig. 14.

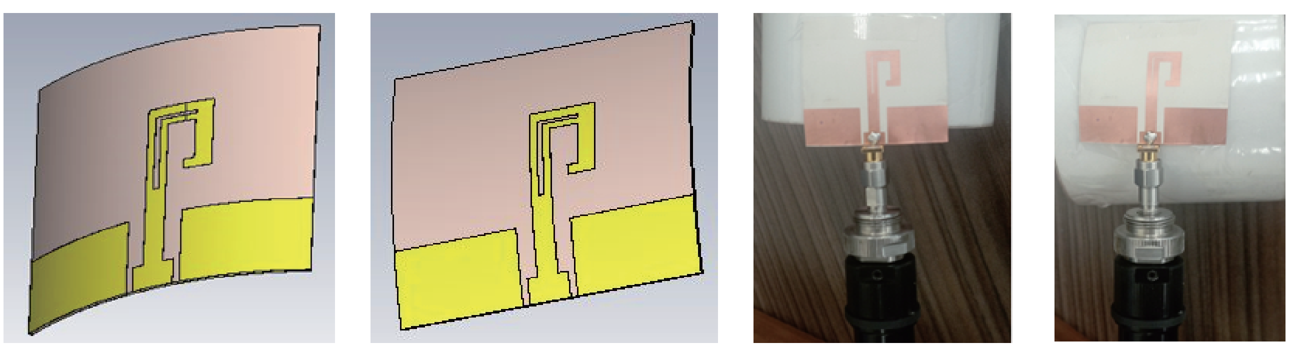

(a) (b) (c) (d)

Figure 11. Antenna design subjected to bending in (a) vertical (simulation) (b) horizontal (simulation) (c) vertical (measurement) (d) horizontal (measurement).

5. HUMAN BODY LOADING ON THE ANTENNA PERFORMANCE

The section focuses on the antenna's performance for close proximity to the human physique. The investigation considered the effect of human multilayer tissue. To assess this, CST MWS software was

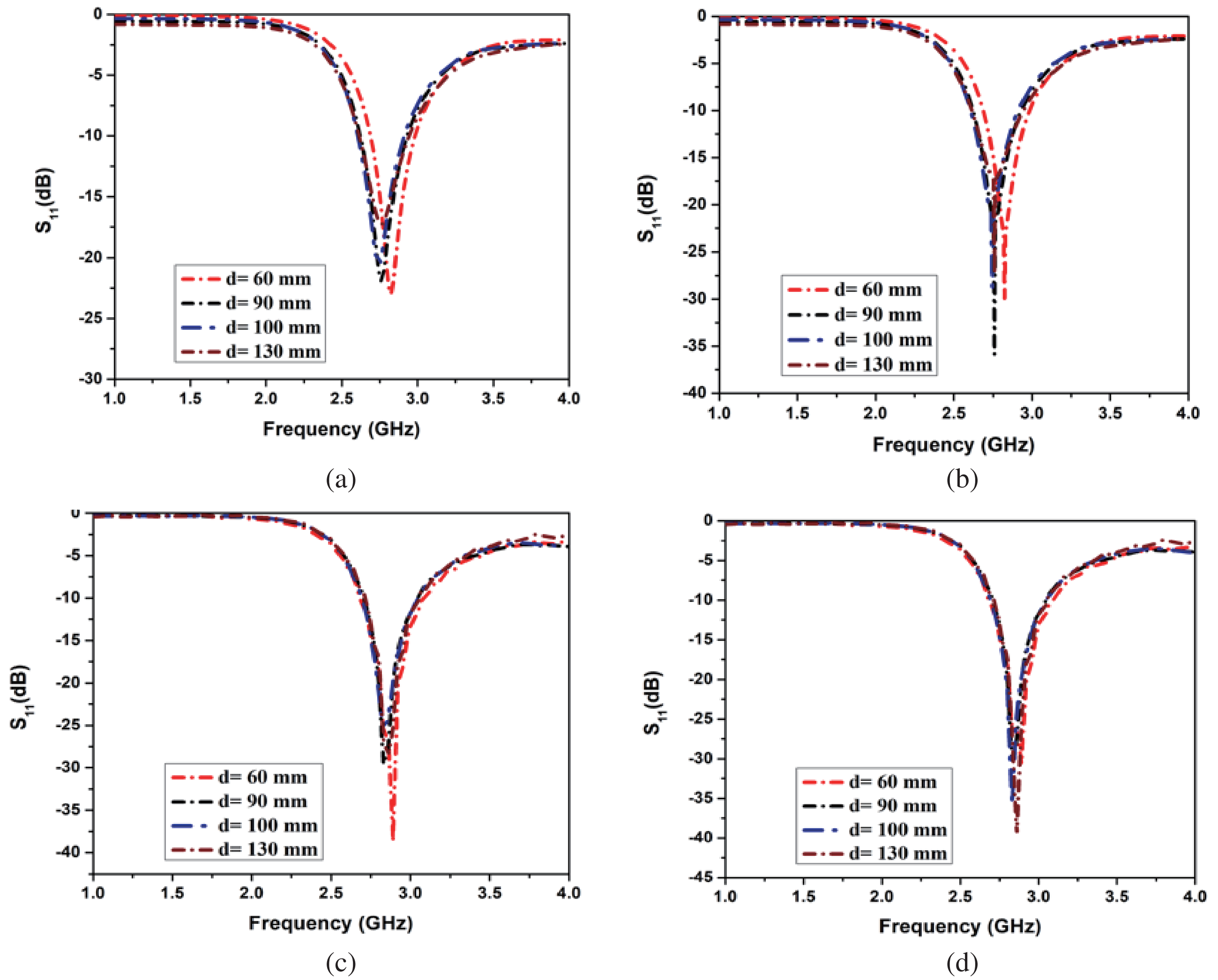

Figure 12. Antenna performance under bending conditions (a) vertical direction (simulated) (b) horizontal direction (simulated) (c) vertical direction (measured) (d) horizontal direction (measured).

used for the numerical simulations. Fig. 15 displays the S_{11} of the antenna under simulation when it was placed on different thicknesses of garments ranging from 1 mm to 3 mm. The presence of a human physique, with high dielectric, affects the antenna's performance. Specifically, note the resonance at 2.3 GHz. Furthermore, the antenna was loaded on various locations of a realistic human model, namely the chest, leg, and bare skin, as illustrated in Figs. 16(a)–(c). The antenna's performance in these scenarios was also analyzed. The measured S_{11} can be observed in Fig. 17, revealing a slight shift in the S_{11} placing the antenna in direct contact with the skin. This shift can be aligned to the high dielectric of human tissue, affecting the resonant frequency. However, Nonetheless, the effect of the human body's influence on the radiation pattern of the antenna, as depicted in Figs. 18(a) and (b), was found to be negligible. The gain of the antenna exhibited a reduction ranging from 2.5 dBi to 3.3 dBi, owing to the high absorption properties of human tissue, as shown in Fig. 19.

6. SAR ANALYSIS

In the process of designing an antenna for medical applications, it is crucial to evaluate the SAR with the antenna's close proximity to the human physique. Compliance with SAR limits is essential, and the standards set by the FCC and ICNIRP state that SAR must not go beyond 1.6/2 W/kg per 1/10 g of

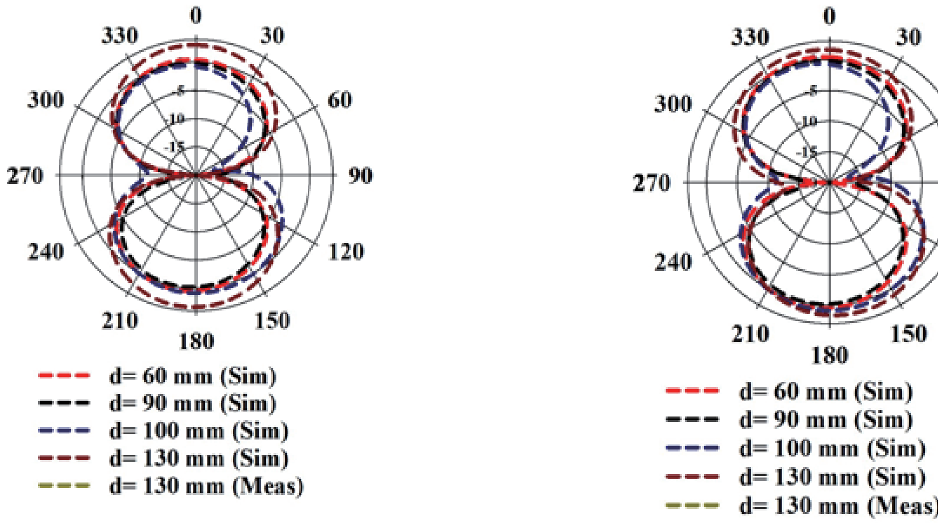

(a) (b)

Figure 13. The radiation pattern under bending (a) vertical direction (b) horizontal direction.

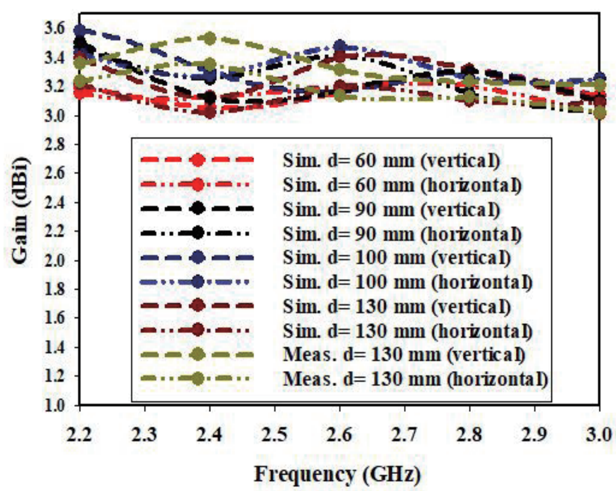

Figure 14. Gain under different bending in the vertical and horizontal direction.

tissue respectively [36, 37]. To calculate SAR values, the IEEE C95.1 standard in CST MWS® software is utilized, using 100 mW input power. Additionally, Figs. 20(a) and (b) illustrate a simplified human body tissue model for the chest and thigh's four layers, namely skin, tissue, muscles, and bones. The depth and information used in this investigation were obtained from [3, 7].

Figures 21 and 22 illustrate the SAR values when wearable antennas are positioned on the chest and thigh, respectively. According to Figs. 21(a) and (b), the SAR values for 1/10 g of human tissue on the chest are 0.018/0.013 W/kg, respectively. Additionally, Figs. 22(a) and (b) demonstrate that the SAR values on the thigh are 0.02/0.015 W/kg for 1/10 g of human tissue, respectively. Consequently, these findings indicate that the SAR values obtained comply with the standards set by the FCC and ICNIRP.

Table 1 presents a comparative analysis between the antenna proposed in this study and the antennas discussed in prior studies. The findings show that the suggested antenna exhibits significantly smaller dimensions than antennas utilized in previous works. Moreover, the antenna demonstrates acceptable impedance bandwidth, SAR, and gain performance in the resonant frequency. The

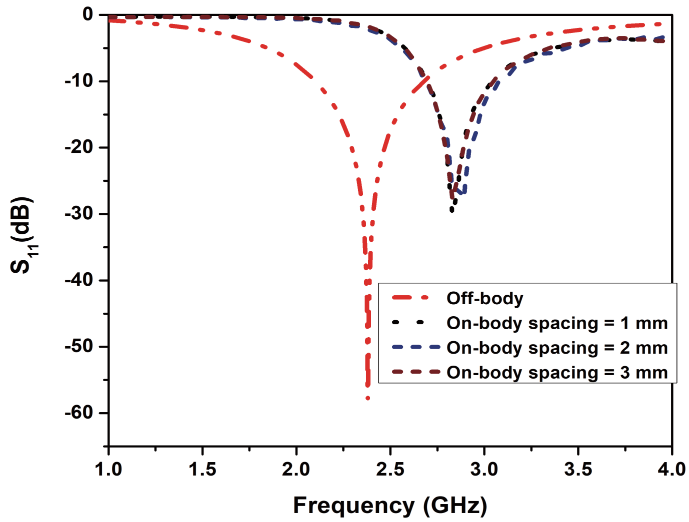

Figure 15. Simulated S_{11} findings for various human clothing levels of thickness.

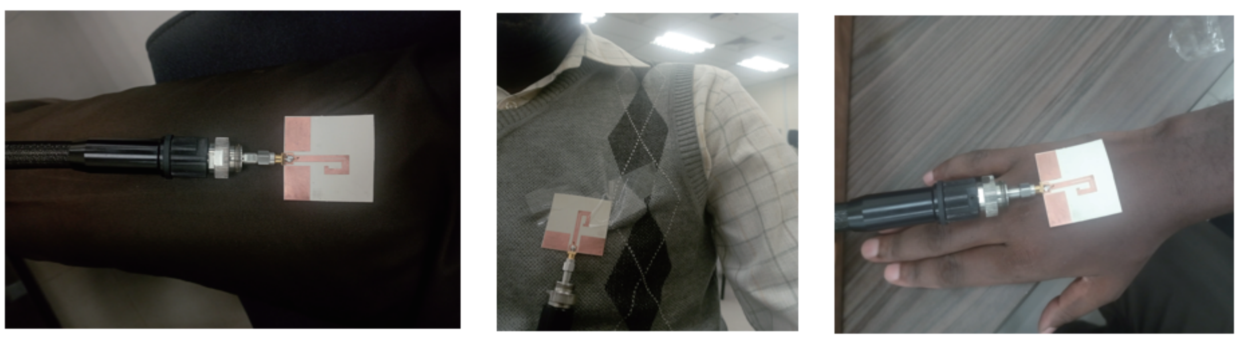

(a) (b) (c)

Figure 16. Prototyped antenna on (a) thigh (b) chest (c) bare skin.

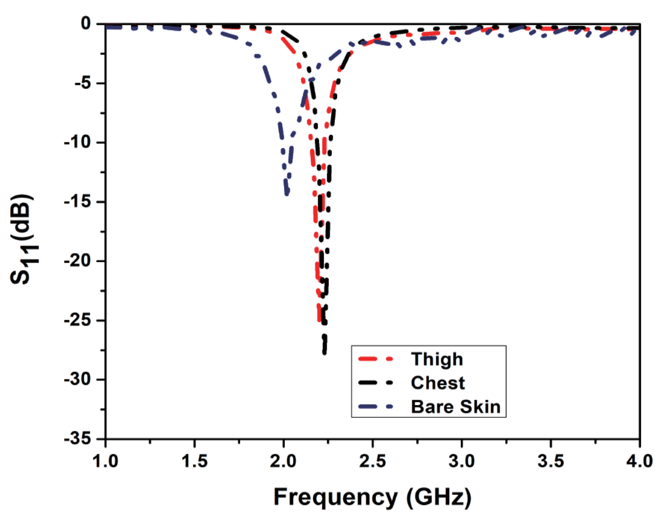

Figure 17. Measured S_{11} on thigh, chest, and bare skin.

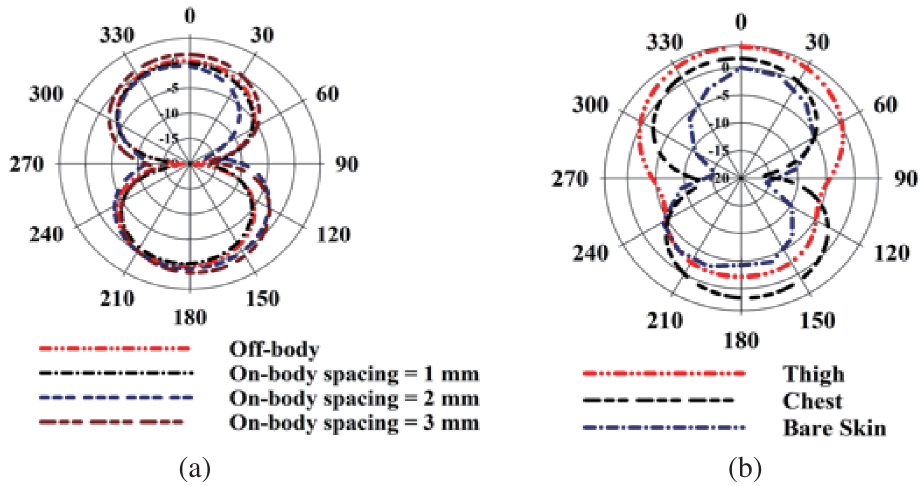

Figure 18. Radiation patterns on the human body (a) simulated (b) measured.

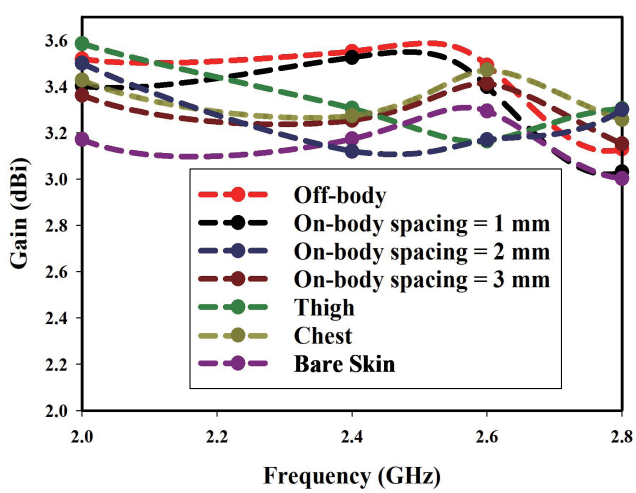

Figure 19. The gain of the antenna simulated and measured on human body.

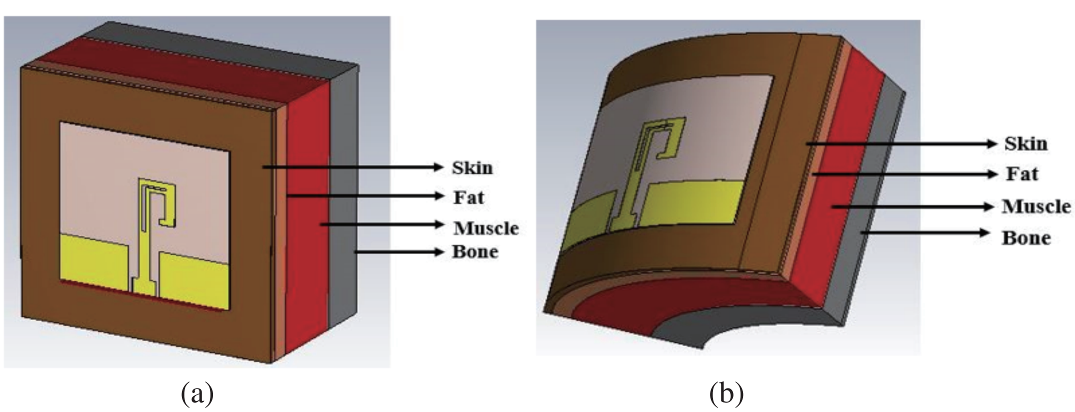

Figure 20. The simplified human body tissue model.

table, clearly shows that the suggested antenna possesses numerous benefits compared to antennas implemented from the prior studies.

Table 1. Performance comparison of the proposed antenna with the antennas used in previous studies.

Ref.	Size (mm^3)	Material	Frequency (GHz)	Bandwidth (%)	SAR (W/kg)	Gain (dBi)	Efficiency (%)
[8]	$45 \times 45 \times 2.4$	Jeans fabric	2.4	-	0.026/0.036	1.96	71.8
[28]	$39 \times 39 \times 0.5$	Rogers	2.4	7.8	1.95/1.56	2.06	75
[38]	$40 \times 35 \times 0.6$	Paper	2.4	8	-	2	83
[39]	$30 \times 20 \times 0.7$	Denim	2.4	15	-	2.05	79
[40]	$46 \times 46 \times 2.4$	Denim	2.4	27	0.04/0.014	7.8	-
[41]	$60 \times 60 \times 2.4$	Jeans fabric	2.4	32.1	0.983/0.258	6.45	-
[42]	$40 \times 32 \times 2$	PDMS	2.4	16.6	0.05/0.03	2.1	90
[43]	$45 \times 35 \times 2.5$	PDMS	2.4	19.2	0.61/0.33	6.56	70
[44]	$50.7 \times 25.7 \times 3$	Felt	2.4	-	0.52/0.41	4.06	44.4
This work	$35 \times 32 \times 0.5$	**Rogers**	2.4	25.2	0.018/0.013	3.54	91

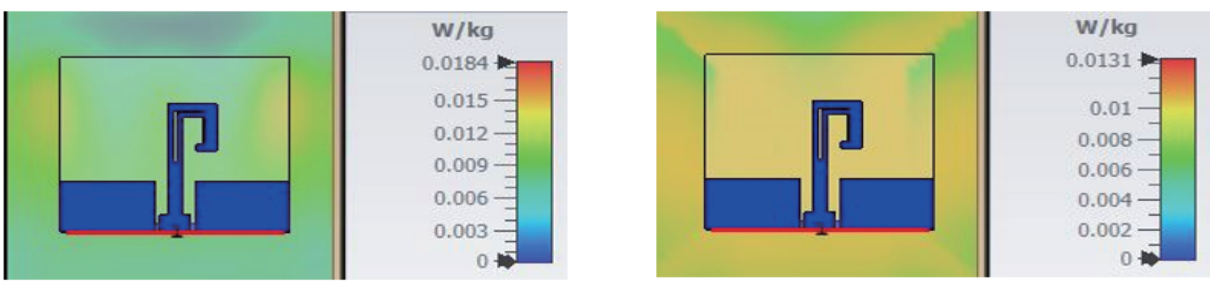

(a) (b)

Figure 21. SAR value with human body tissue model for chest (a) 1 g (b) 10 g (input power of 100 mW).

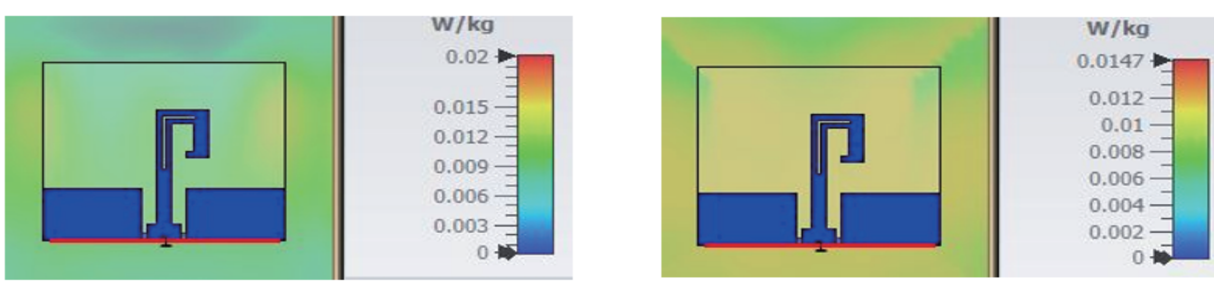

(a) (b)

Figure 22. SAR value with human body tissue model for thigh (a) 1 g (b) 10 g (input power of 100 mW).

7. CONCLUSION

A compact wearable antenna designed specifically for medical applications was presented. The antenna was created using a flexible Rogers Duroid RO3003^{TM} material, resulting in a small form factor measuring $35 \times 32 \times 0.5\,\text{mm}^3$. Initially, a basic P-shaped rectangular patch antenna was used in the design process. However, in the first iteration (Design 1), the antenna exhibited a single resonance around 1.2 GHz, although it was not optimally matched at that frequency. To address this issue and achieve miniaturization, two rectangular patches were introduced beneath the radiating elements, resulting in a modified antenna referred to as Design 2. To further enhance its performance, an inverted L-slot was incorporated. The suggested antenna resonates at 2.4 GHz, with a bandwidth measuring 25.2% and ranging from (2.087–2.692) GHz. The measured radiation patterns demonstrate bidirectional properties in the E-plane and omnidirectional properties in the H-plane and maintain a high gain of 3.54 dBi and an efficiency of 91%. The SAR values are 0.018/0.013 Watt/kg on the chest. Similarly, the SAR values are 0.02/0.015 Watt/kg on the thigh, using 1/10 g of human tissue, which comply with the standards set by the FCC and the ICNIRP. The evaluation of bending and on-body investigation performed indicates that its performance remains unchanged. This conclusively establishes that the antenna possesses the essential capabilities for effective utilization in medical applications.

REFERENCES

1. Abdel Aziz, A. A., A. T. Abdel-Motagaly, A. A. Ibrahim, W. M. A. El Rouby, and M. A. Abdalla, "A printed expanded graphite paper based dual band antenna for conformal wireless applications," *AEU — Int. J. Electron. Commun.*, Vol. 110, 152869, 2019.
2. Yalduz, H., T. E. Tabaru, V. T. Kilic, and M. Turkmen, "Design and analysis of low profile and low SAR full-textile UWB wearable antenna with metamaterial for WBAN applications," *AEU — Int. J. Electron. Commun.*, Vol. 126, 153465, 2020.
3. Musa, U., S. M. Shah, H. A. Majid, et al., "Design and analysis of a compact dual-band wearable antenna for WBAN applications," *IEEE Access*, Vol. 11, 30996–31009, 2023.
4. Mao, C., P. L. Werner, D. H. Werner, D. Vital, and S. Bhardwaj, "Dual-polarized armband embroidered textile antenna for on-/off-body wearable applications," *2019 IEEE International Symposium on Antennas and Propagation and USNC-URSI Radio Science Meeting*, 1555–1556, 2019.
5. Montero, R., C. Camacho-Gómez, P. Espí, and S. Salcedo-Sanz, "Optimal design of a planar textile antenna for industrial scientific medical (ISM) 2.4 GHz wireless body area networks (WBAN) with the CRO-SL algorithm," *Sensors*, Vol. 18, 1982, 2018.
6. Yadav, A., V. Singh, G. Marques, B. Zapirain, and I. La Torre Díez, "Wireless body area networks: UWB wearable textile antenna for telemedicine and mobile health systems," *Micromachines*, Vol. 11, 2020.
7. Biswas, A. K. and U. Chakraborty, "Investigation on decoupling of wide band wearable multiple-input multiple-output antenna elements using microstrip neutralization line," *Int. J. RF Microw. Comput. Eng.*, Vol. 29, No. 7, e21723, 2019.
8. Ashyap, A. Y. I., et al., "Fully fabric high impedance surface-enabled antenna for wearable medical applications," *IEEE Access*, Vol. 9, 6948–6960, 2021.
9. Kumar Biswas, A., S. S. Pattanayak, and U. Chakraborty, "Evaluation of dielectric properties of colored resin plastic button to design a small MIMO antenna," *IEEE Trans. Instrum. Meas.*, Vol. 69, No. 11, 9170–9177, 2020.
10. Basir, A., A. Bouazizi, M. Zada, A. Iqbal, S. Ullah, and U. Naeem, "A dual-band implantable antenna with wide-band characteristics at MICS and ISM bands," *Microw. Opt. Technol. Lett.*, Vol. 60, No. 12, 2944–2949, 2018.
11. Bahrouni, M., et al., "Modeling of a compact, implantable, dual-band antenna for biomedical applications," *Electronics*, Vol. 12, No. 6, 2023.
12. Salama, S., D. Zyoud, and A. Abuelhaija, "Design of a dual-band planar inverted F-L implantable antenna for biomedical applications," *J. Phys. Conf. Ser.*, Vol. 1711, No. 1, 12002, Nov. 2020.

13. Savcı, H. and F. Kaburcuk, "FDTD-based SAR calculation of a wearable antenna for wireless body area network devices," *Int. J. Microw. Wirel. Technol.*, 1–7, 2022.
14. Savcı, H., S. Khan, and F. Kaburcuk, "Analysis of a compact multi-band textile antenna for WBAN and WLAN applications," *Journal*, Vol. 9, No. 3, 255–260, 2021.
15. Suneetha, R. and P. V Sridevi, "Wearable patch antennas on Fr4, rogers and jeans fabric substrates for biomedical applications," *Communication and Intelligent Systems*, 735–743, 2022.
16. Panda, S., A. Gupta, and B. Acharya, "Wearable microstrip patch antennas with different flexible substrates for health monitoring system," *Mater. Today Proc.*, Vol. 45, 4002–4007, 2021.
17. Yan, S., L. A. Y. Poffelie, P. J. Soh, X. Zheng, and G. A. E. Vandenbosch, "On-body performance of wearable UWB textile antenna with full ground plane," *2016 10th European Conference on Antennas and Propagation (EuCAP)*, 1–4, 2016.
18. Mohandoss, S., S. K. Palaniswamy, R. R. Thipparaju, M. Kanagasabai, B. R. Bobbili Naga, and S. Kumar, "On the bending and time domain analysis of compact wideband flexible monopole antennas," *AEU — Int. J. Electron. Commun.*, Vol. 101, 168–181, 2019.
19. Gao, G.-P., C. Yang, B. Hu, R.-F. Zhang, and S.-F. Wang, "A wearable PIFA with an all-textile metasurface for 5 GHz WBAN applications," *IEEE Antennas Wirel. Propag. Lett.*, Vol. 18, No. 2, 288–292, Feb. 2019.
20. Kaur, H. and P. Chawla, "Design and evaluation of a fractal wearable textile antenna for medical applications," *Wirel. Pers. Commun.*, Vol. 128, No. 1, 683–699, 2023.
21. Poonkuzhali, R., Z. Alex, and T. Balakrishnan, "Miniaturized wearable fractal antenna for military applications at VHF band," *Progress In Electromagnetics Research C*, Vol. 62, 179–190, 2016.
22. Tong, X., C. Liu, H. Guo, and X. Liu, "A triple-mode reconfigurable wearable repeater antenna for WBAN applications," *Int. J. RF Microw. Comput. Eng.*, Vol. 29, e21615, 2019.
23. Hong, Y., J. Tak, and J. Choi, "An all-textile SIW cavity-backed circular ring-slot antenna for WBAN applications," *IEEE Antennas Wirel. Propag. Lett.*, Vol. 15, 1995–1999, 2016.
24. Arif, A., M. Zubair, M. Ali, M. U. Khan, and M. Q. Mehmood, "A compact, low-profile fractal antenna for wearable on-body WBAN applications," *IEEE Antennas Wirel. Propag. Lett.*, Vol. PP, 2019.
25. Li, Y. J., Z. Y. Lu, and L. S. Yang, "CPW-fed slot antenna for medical wearable applications," *IEEE Access*, Vol. 7, 42107–42112, 2019.
26. Ayd, A., R. Saad, W. M. Hassan, and A. A. Ibrahim, "A monopole antenna with cotton fabric material for wearable applications," *Sci. Rep.*, Vol. 13, No. 1, 7315, 2023.
27. Kapetanakis, T. N., C. D. Nikolopoulos, K. Petridis, and I. O. Vardiambasis, "Wearable textile antenna with a graphene sheet or conductive fabric patch for the 2.45 GHz band," *Electronics*, Vol. 10, No. 21, 2021.
28. Shah, A. and P. Patel, "Suspended embroidered triangular e-textile broadband antenna loaded with shorting pins," *AEU — Int. J. Electron. Commun.*, Vol. 130, 153573, 2021.
29. Arulmurugan, S., T. R. Sureshkumar, and Z. C. Alex, "Compact wearable microstrip patch antenna for 2.4 GHz using loaded slits and shorting pins," *2021 Emerging Trends in Industry 4.0 (ETI 4.0)*, 1–5, 2021.
30. Agneessens, S., S. Lemey, T. Vervust, and H. Rogier, "Wearable, small, and robust: The circular quarter-mode textile antenna," *IEEE Antennas Wirel. Propag. Lett.*, Vol. 14, 1, 2015.
31. Casula, G. A., "A quarter mode SIW antenna for short-range wireless communications," *Journal of Electromagnetic Waves and Applications*, Vol. 33, No. 7, 853–864, 2019.
32. Sugunavathy, S., V. Sudha, and D. Parthiban, "Fabric woven textile antenna for medical applications," *J. Phys. Conf. Ser.*, Vol. 1917, 12022, 2021.
33. Abolade, J. O., D. B. O. Konditi, and V. M. Dharmadhikary, "Comparative study of textile material characterization techniques for wearable antennas," *Results Mater.*, Vol. 9, 100168, 2021.
34. Suraya, A. N., et al., "Wearable antenna gain enhancement using reactive impedance substrate," *Indones. J. Electr. Eng. Comput. Sci.*, Vol. 13, 708–712, 2019.
35. Hirtenfelder, F., "Effective antenna Simulations using CST Microwave Studio (R)," 239, 2007.

36. International Commission on Non-Ionizing Protection, "Guidelines for limiting exposure to time-varying electric magnetic, and electromagnetic fields (up to 300 GHz)," *Health Phys.*, Vol. 74, No. 4, 494–522, 1998.
37. C95.1 Edition-1999, "IEEE standard for safety levels with respect to human exposure to radio frequency electromagnetic fields, 3 kHz to 300 GHz," *IEEE*, 1–83, Apr. 1999.
38. Ullah, M. A., M. T. Islam, T. Alam, and F. Bin Ashraf, "Paper-based flexible antenna for wearable telemedicine applications at 2.4 GHz ISM band," *Sensors*, Vol. 18, No. 12, 2018.
39. Ashyap, A. Y. I., Z. Z. Abidin, S. H. Dahlan, et al., "Inverted E-shaped wearable textile antenna for medical applications," *IEEE Access*, Vol. 6, 35214–35222, 2018.
40. Ashyap, A., Z. Z. Abidin, S. H. Dahlan, et al., "Compact and low-profile textile EBG-based antenna for wearable medical applications," *IEEE Antennas Wirel. Propag. Lett.*, Vol. 16, 2550–2553, 2017.
41. Ashyap, A. Y. I., S. H. Dahlan, Z. Z. Abidin, et al., "Robust and efficient integrated antenna with EBG-DGS enabled wide bandwidth for wearable medical device applications," *IEEE Access*, Vol. 8, 56346–56358, 2020.
42. Gao, G., R. Zhang, C. Yang, H. Meng, W. Geng, and B. Hu, "Microstrip monopole antenna with a novel UC-EBG for 2.4 GHz WBAN applications," *IET Microwaves, Antennas Propag.*, Vol. 13, 2019.
43. Gao, G., S. Wang, R. Zhang, C. Yang, and B. Hu, "Flexible EBG-backed PIFA based on conductive textile and PDMS for wearable applications," *Microw. Opt. Technol. Lett.*, Vol. 62, 2020.
44. El Atrash, M., M. Abdalla, and H. El-Hennawy, "A compact flexible textile artificial magnetic conductor-based wearable monopole antenna for low specific absorption rate wrist applications," *Int. J. Wirel. Microw. Technol.*, Vol. 13, 2020.